NASA TECHNICAL NOTE

NASA TN D-5407

C. 1

NASA TN D-5407

A COMPUTER PLOTTING DESCRIPTION OF ION-MOLECULE COLLISIONS WITH LONG-LIVED CAPTURE COMPLEXES

by John V. Dugan, Jr., and James H. Rice

Lewis Research Center
Cleveland, Ohio

NATIONAL AERONAUTICS AND SPACE ADMINISTRATION • WASHINGTON, D. C. • SEPTEMBER 1969

A COMPUTER PLOTTING DESCRIPTION OF ION-MOLECULE COLLISIONS WITH LONG-LIVED CAPTURE COMPLEXES

By John V. Dugan, Jr., and James H. Rice

Lewis Research Center
Cleveland, Ohio

NATIONAL AERONAUTICS AND SPACE ADMINISTRATION

For sale by the Clearinghouse for Federal Scientific and Technical Information
Springfield, Virginia 22151 – CFSTI price $3.00

ABSTRACT

Spiraling in ion-molecule collisions with polarizable and/or polar targets is investigated numerically using computer plotting techniques. Collision orbits and interaction behavior are studied for a range of collision parameters on the IBM 360/67 and 7094 computers with the CDC DD280 plotter. Multiple reflections off a hard-core barrier at small ion-molecule separations occur only in collisions with permanent dipoles. Multiple-reflection times for 2 to 2000 reflections are 10 to 10^3 times longer than times for single reflections. Long multiple-reflection collision times, however, do not mean large capture cross sections; the capture cross-section values are much less than those predicted by the adiabatic theory.

A COMPUTER PLOTTING DESCRIPTION OF ION-MOLECULE COLLISIONS WITH LONG-LIVED CAPTURE COMPLEXES

by John V. Dugan, Jr., and James H. Rice

Lewis Research Center

SUMMARY

The degree to which spiraling occurs in ion-molecule collisions with polarizable and/or polar targets is investigated numerically by means of computer plotting techniques. The collision orbits and ion-molecule interaction behavior are studied for a range of collision parameters by using the IBM 360/67 and 7094 computers with the CDC DD280 plotter. The interaction potential consists of a hard-sphere term plus the attractive polarization and ion-dipole terms. Multiple reflections off the hard-core barrier at small ion-molecule separations (i.e., $r \approx$ the reflection distance r_c) occur only in collisions with permanent dipoles. Simple specular reflection occurs in pure polarizability (Langevin) collisions. No spiraling, as conventionally defined, is observed in the approximately 700 collisions studied. Multiple-reflection times τ_c are 10 to 10^3 times longer than the corresponding values for single reflections. As many as 2000 reflections are observed at r_c values of 1 to 3 Å. Long multiple-reflection collision times, however, do not mean large capture cross sections σ_c; the capture cross-section values are much less than predicted by the adiabatic theory.

INTRODUCTION

Collisions between ions and polarizable molecules have been considered as spiraling encounters since the early paper by Langevin (ref. 1). This view was formulated (ref. 2) from the simple orbit equation without any discussion of the conditions necessary for such spiraling behavior. Results of numerical calculations of capture cross sections for ion - permanent dipole collisions were compared (ref. 3) with cross sections for Langevin (dipole moment, $\mu = 0$) collisions involving hydrochloric acid (HCl) targets. The nature of these collision orbits was also examined. These results showed no significant spiraling for the Langevin test cases in the absence of a repulsive potential.

A recent proposal (ref. 4) of accidental resonance in ion-molecule collisions suggests spiraling behavior to explain very long collision times for charge exchange. This report provides results of a numerical investigation of ion-molecule collisions by means of plotting techniques. Collisions involve both polar and nonpolar molecules. The extent of spiraling is investigated, as well as conditions for reflection of the particles off a repulsive barrier. The nature of the collision complex formed in multiple-reflection captures is treated in some detail. A cursory study of the effects of target geometry on ion-molecule complex formation is also included. All symbols are defined in appendix A. The SI system of units is used throughout except for length where angstroms (1 Å = 10^{-10} m) and energy where electron volts (1 eV = 1.602×10^{-19} J) are employed because of the atomic nature of the problem.

COLLISION MODELS

Langevin Collisions

The interaction between an ion and a polarizable molecule (or atom) is described by the ion-induced dipole potential

$$V(r) = -\frac{\alpha e^2}{2(4\pi\epsilon_0)r^4} \tag{1}$$

where α is the electronic polarizability, e is the electronic charge, and r is the ion-molecule separation. In the following discussion this potential energy term is written in atomic units so the mks conversion factor of $(4\pi\epsilon_0)^{-1}$ will be omitted. This attractive potential leads to an orbit equation (ref. 2) which relates the scattering angle β to the separation r by

$$\beta = \pi - \int_0^{\rho_0} \frac{d\rho}{\sqrt{1 - \rho^2 + \frac{\alpha e^2 \rho^4}{mv^2 b^4}}} \tag{2}$$

where $\rho = b/r$ and ρ_0 is the lower of the two positive roots of the radical in equation (2), if the roots exist. For $b < b_L$ (where b_L is the Langevin critical impact parameter equal to $(2\alpha e^2/\epsilon)^{1/4}$), there is no real root and the orbit is of the spiraling

type. Orbits for $b > b_L$ never approach closer than $r_L = b_L/\sqrt{2}$, and ϵ is the initial relative translational energy of the ion and molecule. Thus the probability of capture C_R drops off abruptly to zero (as a step function) at $b = b_L$. Gioumousis and Stevenson (ref. 5) calculated the cross sections for various ion-molecule reactions by assuming that the critical reaction radius is equal to r_L. They obtained satisfactory agreement with certain experiments. Hamill and his co-workers (refs. 6 and 7) studied the question of reaction probabilities as functions of relative velocity experimentally and obtained results consistent with the calculations of references 3, 8, and 9.

Permanent Dipole Collisions

The ion-dipole contribution to the interaction potential is

$$V(r, \gamma) = - \frac{\mu e \cos \gamma}{4\pi\epsilon_0 r^2} \tag{3}$$

where μ is the dipole moment and γ is the angle between the separation vector and the negative end of the dipole. The sign of the permanent dipole potential naturally changes as the polar molecule rotates. The collision orbits for polar targets are not amenable to the simple spiraling description of equation (2). The probability of capture C_R for such collisions has been calculated as a function of impact parameter at fixed values of relative velocity (refs. 3, 8, and 9). This C_R value is a complicated function of impact parameter compared to the step-function dropoff in capture probability for Langevin collisions.

It is clear that the presence of a permanent dipole is necessary for multiple reflections to occur. In the absence of a dipole, the behavior of the ion-molecule pair is best understood in terms of the effective potential V_{eff}, which can be written

$$V_{eff}(r) = \epsilon\left(\frac{b}{r}\right)^2 - \frac{1}{2}\frac{\alpha e^2}{r^4} \tag{4}$$

The maximum in this potential is at

$$r^*_{min} = \left(\frac{\alpha e^2}{\epsilon}\right)^{1/2} b^{-1} \tag{5}$$

Capture (defined as approach to $r \leq r_c$ in this report) occurs only for $b < b_L$; however, for these trajectories the particles simply reflect and pass back over the barrier at $r = r^*$. The condition for capture for $b < b_L$ is, in fact, that the relative energy ϵ be greater than $\left[2V_{eff}(r^*)\alpha e^2/b^4\right]^{1/2}$. No spiraling is observed in collisions without dipoles (ref. 10) (i.e., pure polarizability collisions). For such collisions ($\mu = 0$), it is concluded in reference 10 that long collision times in charge exchange collisions cannot be explained in terms of spiraling behavior.

The presence of a rotating dipole considerably complicates the effective potential description of the ion-molecule collision. Multiple maxima can be introduced in the effective potential; the location of these maxima changes as the dipole rotates. The height of the potential barrier can shift as well. This rapid time variation of the potential permits trapping of the ion after reflection off the step potential (i.e., multiple reflection can occur). A barrier in the effective potential can be introduced for any $r \geq r_c$.

Collision Times

The question of the duration of collisions has arisen in theoretical predictions of Böhme, Hasted, and Ong for cross sections in charge exchange processes (ref. 4). These reactions include polar and nonpolar targets. It is assumed in reference 4 that the adiabatic theory is a satisfactory description of these collisions. "Adiabatic" in this sense means that the electronic configurations of ion and molecule can adjust as the collision proceeds. They then employ Massey's adiabatic description of the cross section, which says that it reaches a maximum when the collision time τ_c equals the characteristic transition time τ_t. The authors of reference 4 suggest that ion-molecule charge exchange proceeds as an "accidentally resonant" process because spiraling implies long collision times. In the adiabatic approximation, long characteristic transition times imply small transition energies $\Delta E_t \approx 0$ (i.e., resonant collisions). (Since the resonance is not due to symmetry effects, the collisions are termed "accidentally resonant.")

Five of the reactions considered in reference 4 involve the polar target molecules carbon monoxide (CO) and nitric oxide (NO). Both of these targets have relatively small dipole moments, 0.1 and 0.16 Debye units. The present study considers cases of low (CO), intermediate (HCl), and high (methyl cyanide (CH_3CN)) dipole moments. The case of CO can be compared with the predictions of reference 4 for charge exchange cross sections. The NO_2^+ - HCl system was chosen not only as representative of intermediate μ value but because the reduced mass for this pair is identical to the value for the $CH_3CN^+ + CH_3CN$ case.

Repulsive Potential

The numerical trajectory calculations of references 3, 8, and 9 were performed with the induced dipole potential term, permanent dipole term, or both terms. If in the course of the trajectory, pair separations of 1 to 2 Å are achieved, the effects of a repulsive potential become significant. The electronic clouds of ion and molecule overlap at these r values. In these previous studies (refs. 3, 8, and 9), the trajectories were stopped where $r = r_c$ (ion-molecule separations of 1 to 2 Å where repulsive effects occur). In the present study, a hard-sphere potential barrier is simulated by changing the sign of the radial velocity $\dot{r}$ at $r = r_c$. Spiraling is defined as changes in the polar angle θ by π and/or the azimuthal angle φ by 2π. In this report we wish to clearly distinguish spiraling (which does not involve multiple reflection) from a trajectory where multiple reflections result in a circuit of the ion around the molecule.

NUMERICAL TRAJECTORY CALCULATION

Details of the numerical calculation have been described in references 3, 8, and 9. The Lagrangian equations of motion for an ion interacting with a linear polar molecule are given in appendix B. The effects of geometry on capture cross sections for ion-dipole collisions have been discussed in references 8 and 9; the equations of motion are very similar for models of symmetric top molecules (ref. 9). The coordinate systems used in the computer study are shown in figures 1(a) and (b). Molecular constants and collision parameters are given in table I.

TABLE I. - COLLISION PARAMETERS[a, b]

Ion-molecule pair	Electronic polarizability, α, $(Å)^3$	Dipole moment, μ, Debye unit	Reduced mass, m, kg	Moment of inertia, I, $kg\text{-}m^2$
$Ar^+ + CO$	1.95	0.10	2.74×10^{-26}	1.44×10^{-46}
$NO_2^+ + HCl$	2.60	1.08	3.41	.268
$CH_3CN^+ + CH_3CN$	3.80	3.92	3.41	9.12

[a] All collisions were studied for an initial ion-molecule relative velocity $v_o \approx 5\times10^4$ cm/sec; the reflection barrier was located at r_c = 1, 1.5, 2, or 3 Å.

[b] Target rotators were chosen from a distribution at a rotational temperature T_R = 300 K.

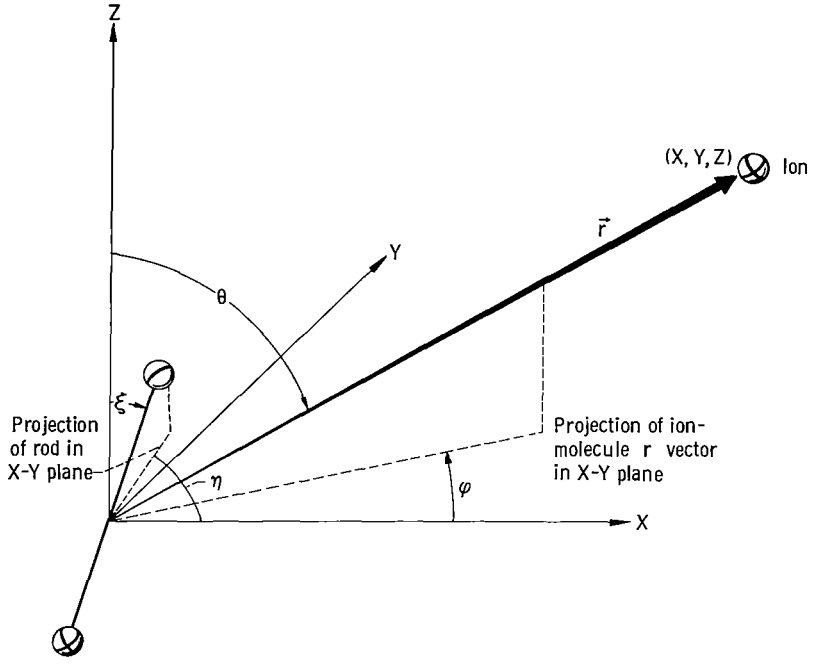

(a) Coordinate system used in computer study of interaction between an ion and a linear polar molecule.

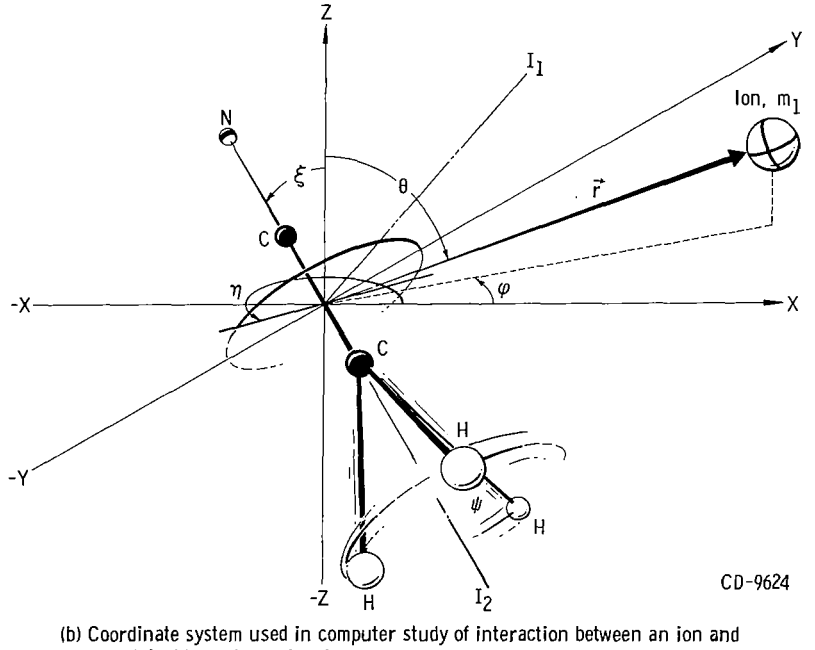

(b) Coordinate system used in computer study of interaction between an ion and symmetrical top polar molecules.

Figure 1. - Coordinate systems used in computer studies of ion-molecule interaction.

Trajectories were started at $r_o = 50$ or 25 Å and continued after interaction until $r \geq r_o$. If the ion-molecule pair reaches a turning point for $r > r_c$ (the "capture" distance), the collision is recorded as a "repulsion." Orbits for which $r \leq r_c$ at any time are denoted "capture" collisions. The step-size changing routine (variable order Runge-Kutta technique) used to integrate the differential equations is described briefly in appendix C.

The collision time τ_c is also of interest for these interactions since according to the adiabatic theorem (refs. 4 and 11) large τ_c implies large reaction cross sections. The choice of interaction distance r* (with τ_c defined as the period for which $r < r^*$) is somewhat arbitrary because of the presence of the dipole. It will be shown, however, that for multiple-reflection collisions the τ_c value is relatively insensitive to the choice of r*. A lower limit to r* (r^*_{min} of eq. (5)) is the maximum in the one-dimensional effective potential for pure polarizability collisions given by equation (4). This potential can be written

$$V_{eff} = \frac{-\alpha e^2}{2r^4} + \frac{L'^2}{2mr^2}$$

where L' is the angular momentum (L' = mvb) and m and v are the reduced mass and relative velocity. An alternative choice of r* is that distance at which translational velocity is first significantly perturbed (~10 percent). This distance varies between 4 to 20 Å for the three collision systems studied. Its value does not differ significantly from the hindering distance r_h (refs. 3 and 8) for representative rotators where r_h is defined by

$$\frac{\mu e}{r_h^2} \approx E_R \tag{6}$$

As long as τ_c is large (i.e., $\tau_c >> \overline{\tau}_o$, the average collision time for a single reflection), the τ_c value remains insensitive to the choice of r*. Capture collisions with $\tau_c \approx \overline{\tau}_o$ are not strictly specular reflections since their orbits are not so simple as in the pure polarizability (Langevin) case. These capture collisions are designated "single-reflection collisions" in the following sections.

COMPUTER PLOTTING APPROACH

The collision trajectories were solved on the IBM 360/67 and 7094 computers and displayed by using the CDC DD280 plotter. The plots of translational motion are done

in a coordinate system where the polar molecule is fixed at the origin. The spherical coordinate angles θ and φ for translational motion were plotted to determine if spiraling behavior occurred. The relative velocity v, rotational energy E_R, rotator projections, orientation angle γ, and ion projections in Cartesian planes could all be plotted so that each feature of the collision could be scanned. Preliminary work on nonreflected trajectories stopped at $r = r_c$ was reported in reference 10. The procedure for plotting and a discussion of running times for multiple-reflection collisions are included in appendix C.

RESULTS AND DISCUSSION

It is of interest to study the nature of multiple reflections as well as the shape of the ion orbits in the field of the dipole. The data for collision times and number of reflections in multiple-reflection captures are included in table II. These data are representative of all the collisions which were studied for the collision parameters given in table I. These results will be discussed in detail after the nature of orbiting and energy exchange have been discussed for all three polar targets.

Collisions of Ar^+ With CO

The variations of polar θ and azimuthal φ angles (for translational motion) with ion-molecule separation for an Ar^+ + CO capture collision are shown in figure 2. The relative velocity is 5×10^4 centimeters per second, corresponding to a relative translational energy $\epsilon \approx 0.03$ electron volt (near thermal). The energy of the rotator in this case was $\approx 0.5\ kT_R$ where $T_R = 300$ K (relatively cold). The initial conditions for all variables and time derivatives are as follows:

Initial conditions:

$r = 25$ Å	$b = 6$ Å
$\theta = 1.571$ rad	$v = 5.5\times10^{-2}$ Å/τ_n
$\varphi = 4.140$ rad	$E_R = 4.99\times10^{-6}\ m_n$ Å$^2/\tau_n^2$
$\eta = 5.870$ rad	$m = 1.44\times10^{-3}\ m_n$
$\xi = 2.511$ rad	

TABLE II. - RESULTS FOR MULTIPLE-REFLECTION COLLISIONS

Ion-molecule pair	Impact parameter, b, Å	Location of reflecting barrier, r_c, Å	Number of cases, n	Langevin potential maximum, r*, Å	Range of numerical interaction radius, defining collision time, Å	Fraction of cases resulting in multiple reflection, f_R	Maximum number of reflections, N_{max}	Average single-reflection time, $\overline{\tau}_o$, sec	Most probable number of multiple reflections, N_M	Average collision time for multiple reflection, $\overline{\tau}_R$, sec	Maximum collision time, τ_{max}, sec
$Ar^+ + CO$	2.0	1.0	33	16.5	5 to 8	0.63	15	1.5×10^{-12}	6	6.0×10^{-12}	1.7×10^{-11}
	3.0	1.5	21	11.0	4 to 8	.13	5	2.5	2	6×10^{-12} to 7×10^{-12}	8.2×10^{-12}
	3.0	3.0	12	11.0	5 to 8	.08	3	$\sim10^{-12}$	3	1.7×10^{-11}	1.7×10^{-11}
	4.0	1.0	24	8.2	4 to 8	.33	18	1.5×10^{-12}	7	4×10^{-12}	8×10^{-12}
	6.0	1.0	49	5.5	4 to 8	.65	42	2.8	8	1.2×10^{-11}	3.5×10^{-11}
	6.0	2.0	23	5.5	5 to 8	.60	54	4	7	$\sim10^{-11}$	2.7
$NO_2^+ + HCl$	4.0	1.0	10	8.5	~10	0.30	1115	1.5×10^{-12}	20	3.3×10^{-11}	7.5×10^{-11}
	4.0	2.0	40	8.5	8 to 12	.10	40	2	4	1.5	3.1
	6.0	1.0	8	5.7	~10	.50	192	2	7	8×10^{-12} to 9×10^{-12}	2
	6.0	2.0	56	5.7	~10	.14	530	1.7	3	5×10^{-12}	6.4
	8.0	1.0	6	4.3	~10	.67	715	4	6	1.6×10^{-11}	5.2
$CH_3CN^+ + CH_3CN$	3.0	3.0	8	13.7	10	0.50	192	2×10^{-12}	7	1.7×10^{-12}	1.7×10^{-11}
	5.0	2.0	33	8.2	15 to 20	.47	[a]25	4	25	1.3×10^{-11}	2
	5.0	3.0	12	8.2	15 to 20	.33	140	4	20	2	8
	6.0	2.0	24	6.5	15 to 20	.46	[a]25	5×10^{-12} to 6×10^{-12}	8	1.8	3.85
	7.0	2.0	24	5.6	15 to 20	.55	[a]25	4×10^{-12}	10	1.6	3.55
	8.0	2.0	12	5.2	15 to 20	.57	40	4.5	8	2	3.75
	10.0	2.0	12	4.1	15 to 20	.57	150	4.5	12	1.5	2.3
	10.0	3.0	12	4.1	15 to 20	.33	40	4.5	15	2	4.9

[a]Case limited to 25 reflections to minimize computer time.

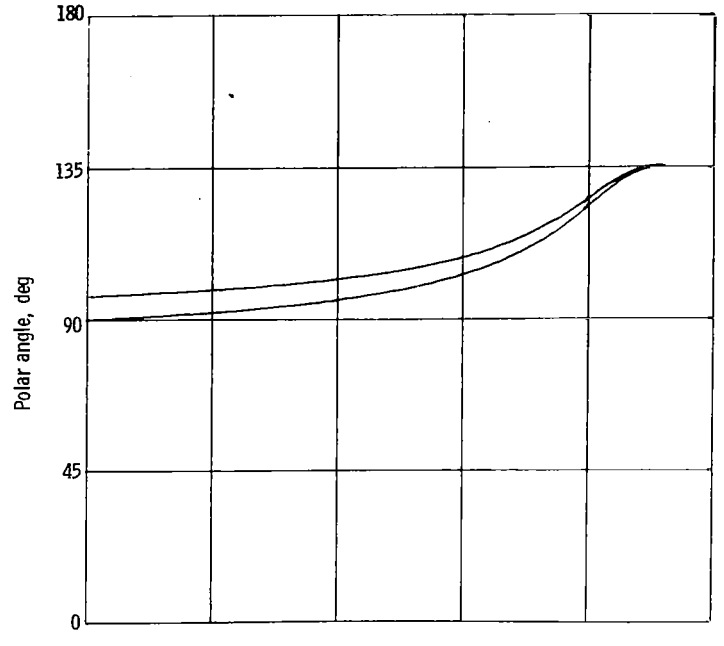

(a) Polar angle, θ.

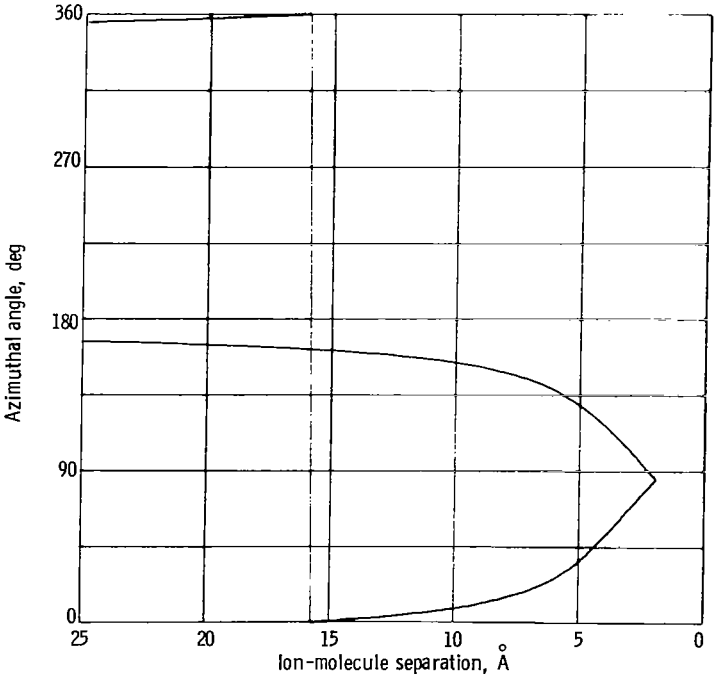

(b) Azimuthal angle, φ.

Figure 2. - Variation of coordinate angles for argon ion (Ar^+) relative to carbon monoxide (CO) molecule during single-reflection capture collision.

Time derivatives:

$$\dot{r} = -5.34\times10^{-2}\ \text{Å}/\tau_n \qquad \dot{\xi} = 4.25\times10^{-2}\ \text{rad}/\tau_n$$

$$\dot{\theta} = 4.65\times10^{-4}\ \text{rad}/\tau_n \qquad \dot{\eta} = 1.63\times10^{-1}\ \text{rad}/\tau_n$$

$$\dot{\varphi} = 2.5\times10^{-4}\ \text{rad}/\tau_n$$

where the scaling values are $\tau_n = 10^{-14}$ second and $m_n = 10^{-20}$ gram (10^{-23} kg). The capture trajectory of figure 2 was solved for an r_c value of 1 Å at an impact parameter of 6 Å. It is a single reflection where the collision time $\tau_o \approx 1.5\times10^{-12}$ second. This is representative behavior for such collisions where the dipole interaction is similar to the polarizability potential for $b \leq b_L$. The collision distance r^* (≈5 Å) was obtained from the plot of translational velocity v against separation distance (i.e., where ϵ is perturbed by 10 percent). The collision time calculated numerically is not very different from $\tau_o \approx 2r^*/v_o \cong 10^{-12}$ second since $r_c << r^*$.

Energy exchange between translational and rotational modes can be conveniently discussed in terms of the relative velocity and translational energy. Figure 3(a) shows the variation of relative velocity v with ion-molecule separation. There is considerable

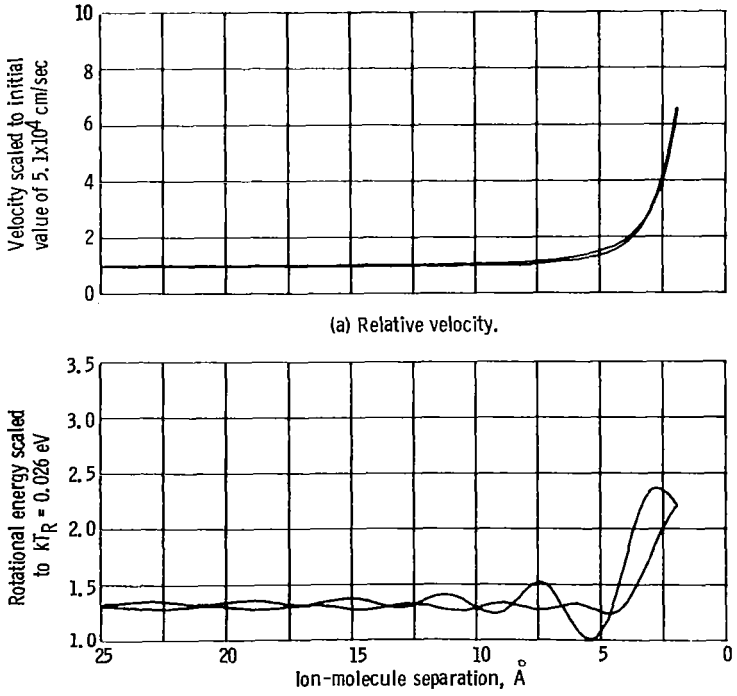

(a) Relative velocity.

(b) Molecular rotational energy.

Figure 3. - Variation of relative velocity and molecular rotational energy during $Ar^+ + CO$ single-reflection capture collision.

acceleration of the translational motion. This acceleration generally occurs within 5 Å. The maximum acceleration is determined by the $\mu e/r^2$ value at $r \approx r_c$. Very little rotational energy seems to have been transformed to the translational mode as the particles return to r_o. Correspondingly, although the rotational energy is usually considerably increased during interaction (as shown in fig. 3(b)), the rotor usually returns to its initial energy state. This behavior is consistent with the experimental condition of a monoenergetic beam of ions with velocity equal to $\sqrt{2kT_R/m}$ incident upon a Maxwellian distribution of rotators at T_R = 300 K (refs. 6 and 7). The oscillatory pattern of variation in rotational energy is characteristic of these ion-dipole collisions. The frequency is inversely proportional to the moment of inertia, except at small r where the variation becomes quite random.

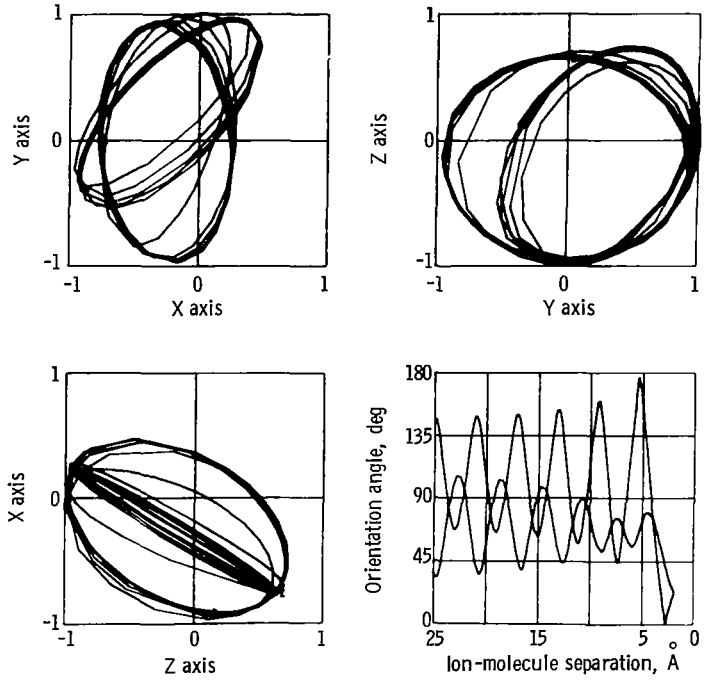

Figure 4. - Variation of rotator projections and orientation angle during Ar^+ + CO single-reflection capture collision.

Figure 4 shows the variation in the rotator projections as the collision proceeds; the curves are not completely smooth because every second point was plotted. The CO target has a moderately large moment of inertia so the rotator trace shows only a modest number of rotations during collision. In several collisions there is evidence of hindered rotation of the dipole by the incident ion (i.e., dipole is preferentially alined with its negative end facing the ion).

Figure 5 shows the interesting orbiting behavior for an Ar^+ + CO capture collision

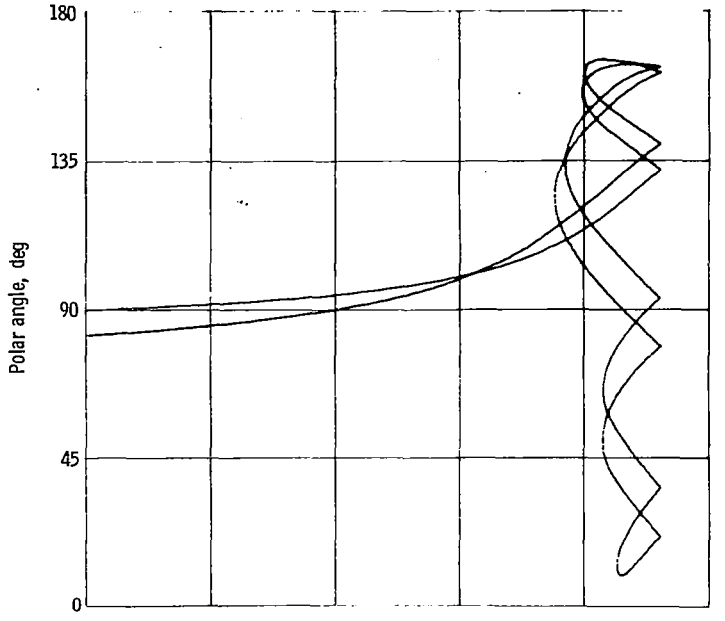

(a) Polar angle, θ.

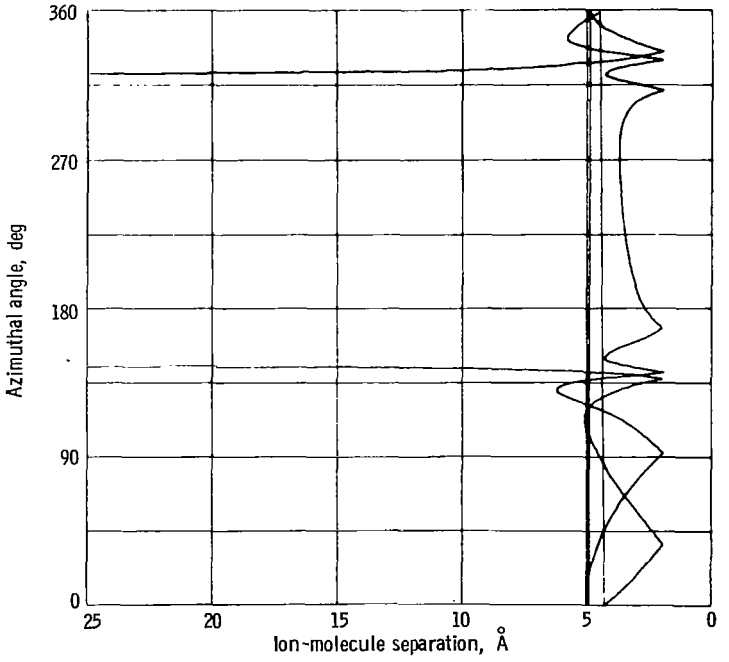

(b) Azimuthal angle, φ.

Figure 5. - Variation of coordinate angles for Ar^+ relative to CO molecule during multiple-reflection capture collision.

where the ion-molecule pair is multiply reflected off a stepwise barrier. This particular encounter resulted in eight reflections. For this critical distance (r_c = 2 Å), as many as 40 or 50 reflections occurred in some cases for CO targets (see table II); however, it is difficult to determine the time history from a θ against r plot with so many reflections.

The maximum b values at which a significant fraction of captures occur are approximately equal to the b_c values where the numerical cross section $\sigma_c \equiv \pi b_c^2$. The σ_c values drop off to quite low values for $v = 2\times10^5$ centimeters per second. There are no multiple-reflection capture collisions observed for CO at this velocity. The ion-molecule relative energy ϵ is so large at these small b values that the dipole term is prevented from introducing reflecting maxima in the effective potential. The σ_c values are approximately equal to σ_L since interaction at the turning points is dominated by the $-\alpha e^2/2r^4$ term. The slope of σ_c against ϵ is roughly $\epsilon^{-1/2}$, however, which is similar to the Langevin prediction for the polarizability potential (ref. 1). A change in slope might be expected if there is a maximum amount of translational energy which can be randomized (absorbed) as internal energy in the ion-molecule complex.

Collisions of NO_2^+ With HCl

Orbiting behavior in a multiple-reflection collision for the system NO_2^+ + HCl is shown in figure 6. The ion-dipole term dominates the interaction here, in contrast to the CO case. The traces do not return to r_o because the plot capacity was exceeded for this case.

The general features of the NO_2^+ + HCl interaction are shown in figure 7. The relative velocity and rotational energy first become perturbed at 5 to 10 Å because the dominant $-\mu e/r^2$ term is significant at these distances. The variations in both v and E_R are similar to the case of CO targets. The heavy structure in the rotator projection plots of figure 8 is a result of the small moment of inertia for HCl, 2.68×10^{-47} kilogram-meter^2. The motion of the rotator is clearly as random as for the CO case, although some hindered rotations are also observed.

Collisions of CH_3CN^+ With CH_3CN

Multiple-reflection behavior for CH_3CN targets is shown in figure 9 by means of the variation of polar and azimuthal angles with ion-molecule separation. The striking characteristic of these capture collisions is the large values at which the turning points occur for multiple reflections. The maximum observed turning-point value is 22 Å. The reflections in figures 9(a) and (b) have a maximum turning point at about 10 Å. Figure 10 shows the case of double minima where the large dipole moment introduces turning points

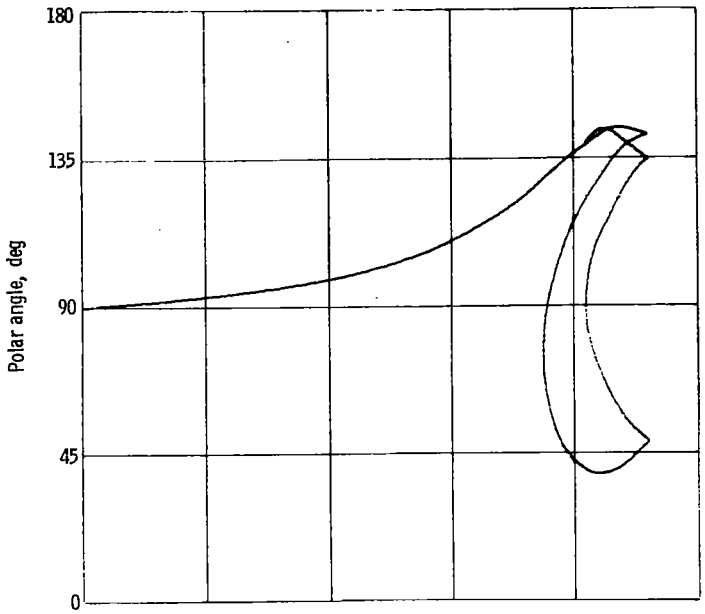

(a) Polar angle, θ.

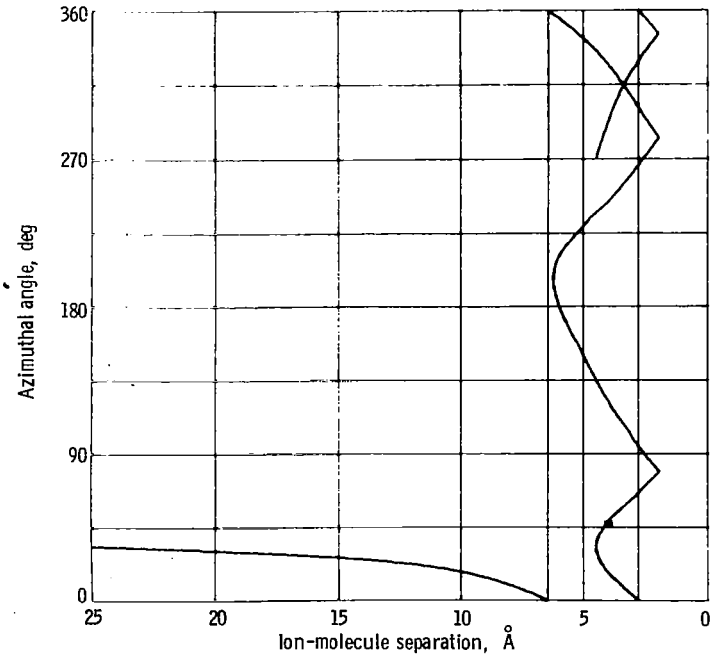

(b) Azimuthal angle, φ.

Figure 6. - Variation of coordinate for nitrogen dioxide ion (NO_2^+) relative to hydrochloric acid (HCl) molecule during multiple-reflection capture collision.

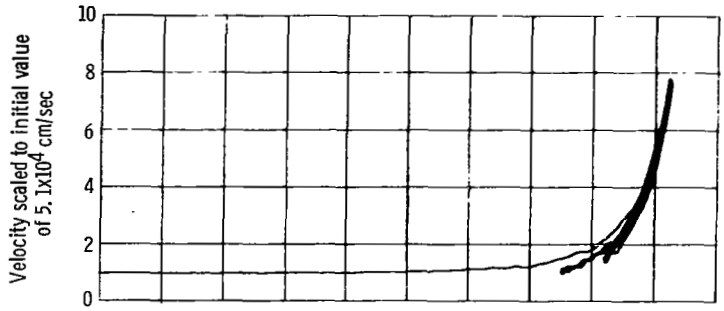

(a) Relative velocity.

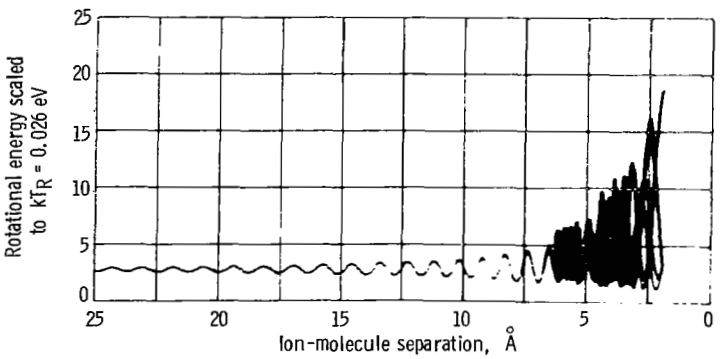

(b) Molecular rotational energy.

Figure 7. - Variations of relative velocity and molecular rotational energy during NO_2^+ + HCl multiple-reflection capture collision.

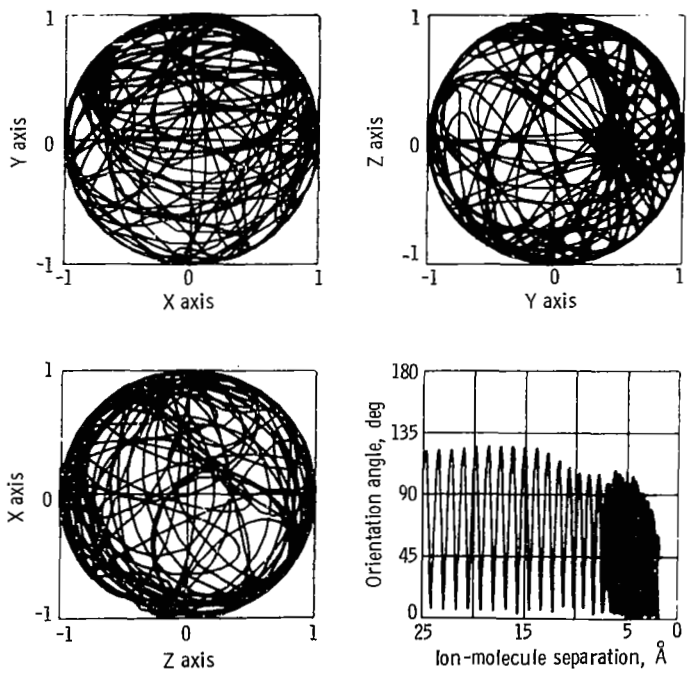

Figure 8. - Variations of rotator projections and ion-molecule orientation angle during NO_2^+ + HCl multiple-reflection capture collision.

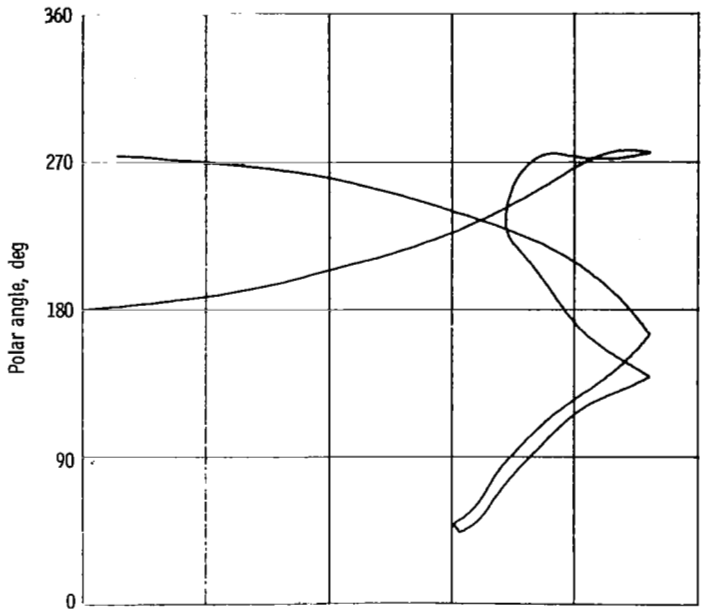

(a) Polar angle, θ.

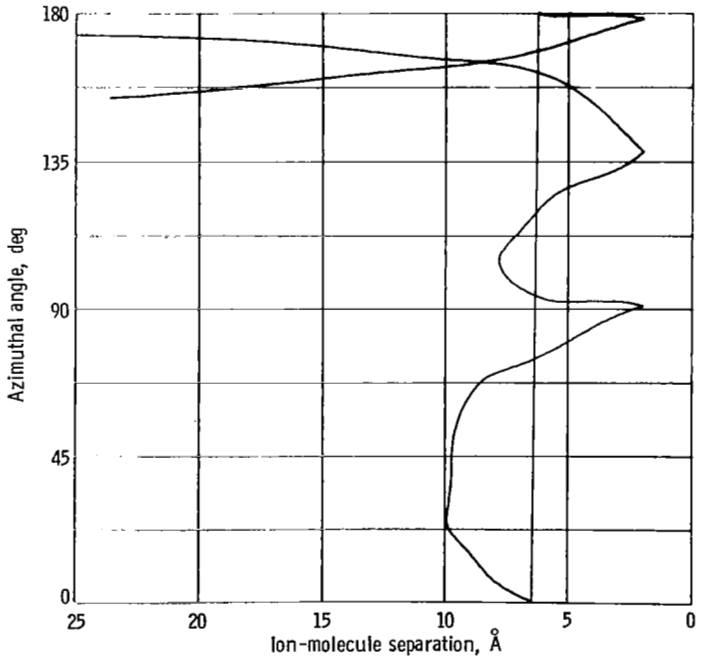

(b) Azimuthal angle, φ.

Figure 9. - Variation of coordinate angles for methyl cyanide parent ion relative to CH_3CN molecule for multiple-reflection capture collision.

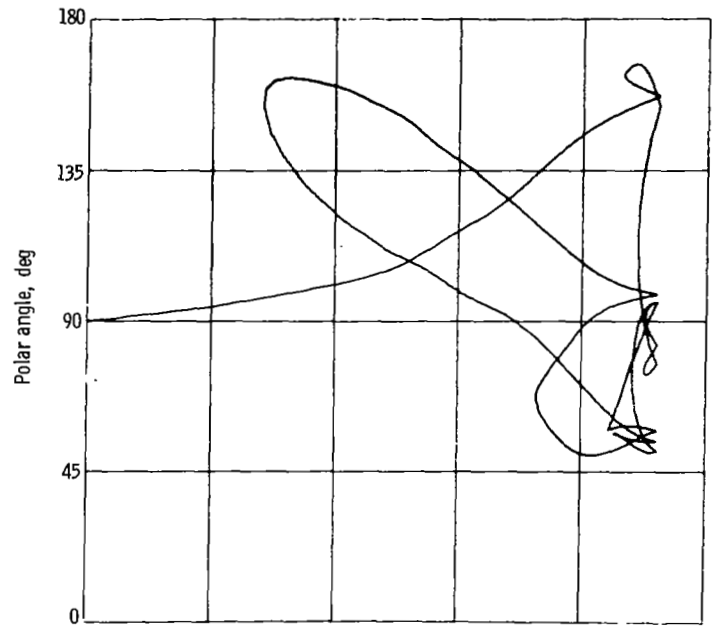

(a) Polar angle, θ.

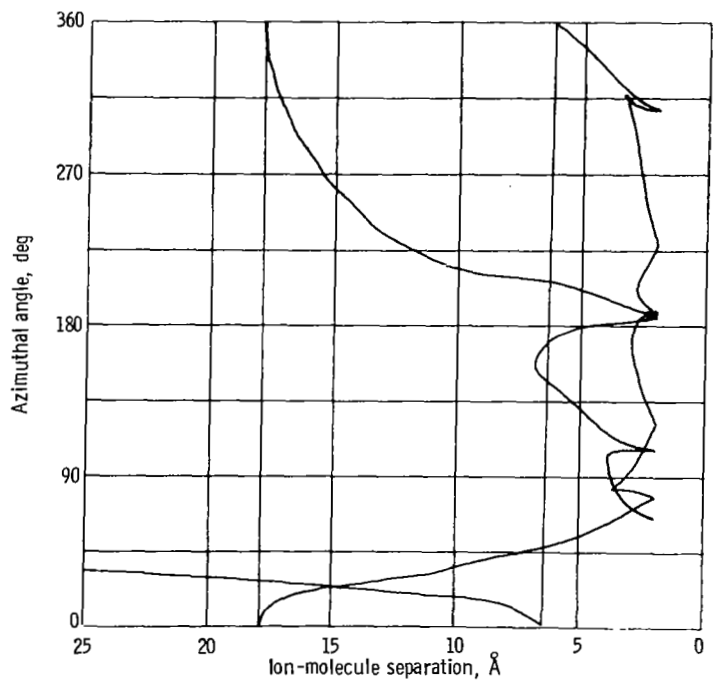

(b) Azimuthal angle, φ.

Figure 10. - Variation of coordinate angles for methyl cyanide parent ion relative to CH_3CN molecule during multiple-reflection capture collision with double minima.

at 2 to 6 Å and at 18 Å.

Again the features of the v and E_R variation are similar to other targets; yet because of the large μ value, interaction begins at large r. Because of the large moment of inertia for CH_3CN (five times the CO value), there are usually relatively few traces in the rotator projection plots. However, multiple reflections obscure the time history, and hindered rotation is not readily apparent (see fig. 11). The random (increasing or decreasing) amplitude variation in orientation angle γ is characteristic of all polar targets. Generally, as illustrated in figure 11, the mean value of γ for small separations is between 0^o and 60^o (i.e., the dipole is in an attractive position with respect to the ion.)

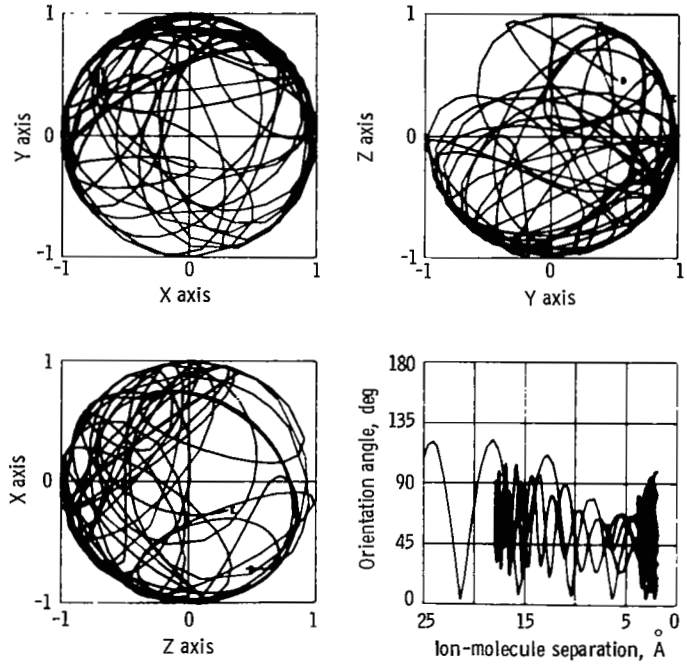

Figure 11. - Variations of rotator projections and ion-molecule orientation angle during $CH_3CN^+ + CH_3CN$ multiple-reflection capture collision with double minima.

Numerical Collision Time Results

Table II includes values of collision times for single- and multiple-reflection collisions, fraction of collisions resulting in multiple reflection, and mean times and reflection numbers for multiple-reflection collisions. Each set of cases consisted of the indicated number of randomly generated cases at a fixed impact parameter. The most probable number N_M and maximum number N_{max} of reflections are also given.

The fraction of capture collisions in which multiple reflections occurred for the 162

Ar^+ + CO cases studied varied from 0.2 to 0.8 at impact parameters from 2 to 6 Å. This fraction falls off abruptly for 6 to 7 Å because the capture cross section is limited to $b_c \approx b_L$. These results are generally true for r_c values of 1 and 2 Å. For large r_c values (3 to 4 Å), there are no reflections in the range of interesting b values since the interaction is dominated by the polarizability potential at the turning points. It should be noted that long collision times $\tau_c >> \tau_o$, which are observed, do not imply large cross sections σ_c. The capture cross section for CO and NO_2 targets is approximately the Langevin cross section independent of the occurrence of multiple reflections. The characteristic radii (turning points) of the ion-molecule collision complex for Ar^+ + CO are 3 to 6 Å (ref. 10).

Single-reflection times for HCl targets are approximately equal to the CO values at the same velocities (see table II). However, HCl target collisions usually show many more reflections than CO targets. This is partly due to the small moment of inertia for HCl (i.e., high rotational frequency). Also the high dipole moment causes a stronger interaction with larger changes in E_R value. Table II allows for a comparison of collision times for multiple and single reflections involving CO (μ = 0.1 Debye unit) and HCl (μ = 1.08 Debye unit). It is clear that the $\bar{\tau}_R$ values are generally larger for HCl (compared to CO) at r_c values of 1 and 2 Å. The characteristic radius r_t of the $HCl+NO_2^+$ complex, ≈5 Å, is slightly larger than for Ar^+ + CO because the higher dipole moment of HCl introduces potential maxima at larger r values. The variation in ion velocity is such that the collision time cannot be simply computed from the number of reflections with the initial velocity value.

It is not clear why the multiple-reflection behavior for HCl is strongly dependent on r_c value. Also interesting but not explainable for the NO_2^+ + HCl collisions is the very large number of multiple reflections that occur for some cases; it appears that, once trapped, the ion finds it very difficult to escape from the HCl molecule.

The τ_c values for multiple-reflection CH_3CN collisions are generally large compared to single-reflection times but not quite as large as the corresponding τ_c values for HCl targets. The fraction of capture collisions which result in specular reflection is relatively large for CH_3CN collisions with r_c values of 1 and 2 Å and remains significant even for r_c = 3 Å. It is noteworthy that this complex has a characteristic radius which is considerably larger than molecular bond distances. It would certainly be of interest to calculate charge transfer probabilities for these collisions since the heavy-particle motion has been calculated. The capture cross section for CH_3CN targets (ref. 9) is approximately equal to the area described by the orbit radius b_c of 12 to 15 Å. These capture cross-section values $\left(\sigma_c \equiv \pi b_c^2\right)$ are approximately 1000 square angstroms at thermal energy.

CONCLUDING REMARKS

The approximation of a classical ion-dipole plus ion-induced dipole (polarizability) potential has been used with a hard-sphere reflecting barrier to study collisions. With this approach, it has been demonstrated that spiraling (as distinguished from multiple reflections) of collision partners does not occur over the wide range of collision parameters studied. Multiple reflections off a repulsive barrier do occur but only for collisions with polar targets. The fraction of multiple-reflection collisions depends on the hard-sphere radius r_c and the electrical properties of the target atom (i.e., polarizability and dipole moment). The CO molecule represents the limit of small μ (0.10 Debye unit) when the polarizability term dominates the interactions. The capture cross section in this case is approximately Langevin, but the dipole still causes multiple reflection to be probable if $r_c \leq 2$ Å. The CH_3CN molecule is the large dipole moment limit when the ion-dipole term dominates, leading to large σ_c values ($\sigma_c >> \sigma_L$). The probability of multiple-reflection collisions is larger for CH_3CN than for CO as long as $r_c \leq 3$ Å for the former. Collision times for multiple-reflection collisions are longest for HCl, as much as 10^3 times single-reflection times, but the fraction of such collisions for HCl targets is small. The characteristic radii of ion-molecule complexes are large (3 to 22 Å) and generally approximate the critical impact parameters for capture. The presence of the dipole is clearly required for multiple reflection with the mathematical model used. The general features of the collisions (i.e., variation in relative velocity and rotational energy) are similar for all polar targets.

Lewis Research Center,
National Aeronautics and Space Administration,
Cleveland, Ohio, June 5, 1969,
120-26-03-04-22.

APPENDIX A

SYMBOLS

b	impact parameter, Å
b_c	critical impact parameter defining numerical capture cross section, Å
b_L	Langevin critical impact parameter, Å
C_R	capture probability, dimensionless
E_R	rotational energy of polar molecule, eV (1 eV = 1.602×10^{-19} J)
ΔE_t	transition energy for ion-molecule charge transfer, J
e	electronic charge, 1.602×10^{-19} C
F_v'	potential function in translational acceleration expression, Å
k	Boltzmann constant, 1.381×10^{-23} J/K
L	Lagrangian energy expression, T - V, eV
L'	translational angular momentum, mvb, kg-m^2/sec
m	reduced mass, kg
q	generalized coordinate
r	ion-molecule separation, Å
r_c	location of hard-core potential, Å
r_h	hindering distance for polar rotation, Å
r_L	distance of closest approach in Langevin collisions, Å
r_o	initial ion-molecule separation, Å
r_t	turning-point radius for ion-molecule collision complex, Å
r^*	numerically computed interaction distance, Å
r^*_{min}	location of maximum in effective polarizability potential, Å
T	kinetic energy of ion-molecule system, rotational plus translational, eV
T_R	rotational temperature of polar molecule targets, K
V	ion-molecule interaction potential energy, eV
V_{eff}	effective one-dimensional potential energy of colliding system, eV
V_o	hard-sphere potential barrier of infinite height

v	relative translational velocity, m/sec
v_o	initial relative translational velocity, m/sec
α	electronic polarizability, $(Å)^3$
β	scattering angle for Langevin collision, rad
γ	orientation angle between dipole and ion-molecule radius vector, rad
ϵ	relative translational kinetic energy, eV
ϵ_o	dielectric permittivity of vacuum, 8.537×10^{-12} farad meter^{-1}
η	azimuthal angle for rotational motion, rad
θ	polar angle for translational motion, rad
μ	permanent electric dipole moment, C-m (1 Debye unit = 3.33×10^{-30} C-m)
ξ	polar angle for rotational motion, rad
ρ	reduced impact parameter (for Langevin collisions $\rho = b/r$), dimensionless
σ	cross section, $(Å)^2$
σ_c	numerical capture cross section, $(Å)^2$
σ_L	Langevin capture cross section, $(Å)^2$
τ	collision time, sec
τ_c	collision time for multiple-reflection collision, sec
τ_o	collision time for single-reflection collision, sec
τ_t	transition time for ion-molecule charge transfer, sec
φ	azimuthal angle for translational motion, rad

APPENDIX B

EQUATIONS OF MOTION AND VALUES OF MOLECULAR CONSTANTS

The Lagrangian energy expression for the ion - linear molecule collision system depicted in figure 1(a) is

$$L = T - V = \frac{m}{2}(\dot{X}^2 + \dot{Y}^2 + \dot{Z}^2) + \frac{I_1}{2}(\dot{\xi}^2 + \dot{\eta}^2 \sin^2\xi)$$

$$+ \frac{\mu e}{r^3}(X \sin\xi \cos\eta + Y \sin\eta + Z \cos\xi) + \frac{\alpha e^2}{2r^4} \tag{A1}$$

where m, I, μ, α, and e are the reduced mass, moment of inertia, dipole moment, electronic polarizability, and electronic charge, respectively. The potential energy term is written in atomic physics units (i.e., substitute $4\pi\epsilon_o$ in denominator to convert to SI units).

The equations of motion are simply

$$\frac{d}{dt}\left(\frac{\partial L}{\partial \dot{q}}\right) - \left(\frac{\partial L}{\partial q}\right) = 0 \tag{A2}$$

where q = X, Y, Z, ξ, and η.

The translational coordinates equations are

$$\ddot{X} = \frac{\mu e}{mr^5}(r^2 \sin\xi \cos\eta - 3XF_V') - \frac{2\alpha e^2 X}{mr^6} \tag{A3}$$

$$\ddot{Y} = \frac{\mu e}{mr^5}(r^2 \sin\xi \sin\eta - 3YF_V') - \frac{2\alpha e^2 Y}{mr^6} \tag{A4}$$

$$\ddot{Z} = \frac{\mu e}{mr^5}(r^2 \cos\xi - 3ZF_V') - \frac{2\alpha e^2 Z}{mr^6} \tag{A5}$$

where the potential function

$$F_V' = X \sin\xi \cos\eta + Y \sin\xi \sin\eta + Z \cos\xi$$

The corresponding rotational coordinate equations are

$$\ddot{\xi} = \eta^2 \sin \xi \cos \xi - \frac{\mu e}{I_1 r^3} (Z \sin \xi + X \cos \xi \cos \eta - Y \cos \xi \sin \eta) \tag{A6}$$

$$\ddot{\eta} = \frac{\frac{\mu e}{r^2} (Y \cos \eta - X \sin \eta) - 2I_1 \eta \xi \cos \xi}{I_1 \sin \xi} \tag{A7}$$

Numerical singularity difficulties caused by the $\sin \xi$ term in the denominator of equation (A7) prevent an accurate calculation of the azimuthal acceleration $\ddot{\eta}$. This singularity is avoided by transforming to a second Euler angle system whose polar axis is orthogonal to that of the first system (refs. 3, 8, and 9). The form of the equations for symmetric top targets (see fig. 1(b)) has been extensively discussed in reference 8.

APPENDIX C

INTEGRATION AND PLOTTING PROCEDURES

The differential equations are integrated by using the variable-step-length Runge-Kutta scheme discussed in appendix C of reference 9. The error introduced in each integration step is estimated by considering the difference between the theoretically conserved total energy $T + V$ before and after the step. If this difference is greater than a specified tolerance (proportional to the step length), the step length is reduced and the integration procedure repeated. However, if the energy difference is less than the specified tolerance, the step is accepted and a new length is computed for the next step.

The initial conditions were generated randomly in the manner described in references 3, 8, and 9. These initial conditions and values at the end of each successful integration step are stored in a plotting array for each of the quantities to be displayed by computer plotting. After the integration is completed, the plotting subroutines are called. Each plotting array contains $N + 1$ values, where N is the number of successful integration steps. A typical range for N is approximately 500 to 1000. For each plot the contents of one array (e.g., coordinate angles, relative velocity, or rotational energy) are taken as ordinate values to be plotted against the abscissa values (usually r, the ion-molecule separation). The consecutive points so determined are then connected by N straight lines. The total energy variation tolerated over the entire integration is usually set at 10^{-4} to 10^{-3}. Standard fourth-order Runge-Kutta and fifth and sixth orders are most often used. The resulting step lengths for these combinations are sufficiently short so as to give acceptably smooth curves. An exception to this regular behavior is observed for unusually low rotational energy cases. The trajectory solutions are also slightly sensitive to step-size histories (i.e., the order in which the trajectories are solved). The number of multiple reflections may change with step-size history, but this is not felt to prejudice the statistical worth of the results.

As noted in reference 9, this integration scheme has yielded more accurate results and significantly shorter computer run times than fixed-step-length routines. For example, the system $Ar^+ + CO$ with a relative translational velocity v of 5.5×10^4 centimeters per second and a rotational energy $E_R \approx kT_R$ for $T_R = 300$ K required an average computer time per case of 10 to 15 seconds, including plotting.

The plotting hardware and the subroutines required to operate it are described in reference 12. The DD280 recorder consists of a cathode-ray display tube and a 35-millimeter still camera. Calls to the plotting subroutine produce images on the display tube, which is an on-line output device to the Lewis IBM 360/67 computer. The 35-millimeter camera photographs the image and advances the film to the next frame.

After developing, the film can be studied in a viewer, printed on photographic paper, or submitted for reproduction in a publication. The plotting subroutines are quite flexible, permitting programmer-designated plot titles, axes labels, point or curve labels, grid selection, plot size and margin adjustment, plots extending over several frames, and multiple plots on a single frame.

REFERENCES

1. Langevin, P.: Une Formule fondamentale de théorie Cinétique. Ann. Chem. Phys., Ser. 8, vol. 5, 1905, pp. 245-288.

2. McDaniel, Earl W.: Collision Phenomena in Ionized Gases. John Wiley & Sons, Inc., 1964, p. 72 and App. II.

3. Dugan, John V., Jr.; and Magee, John L.: Capture Collisions Between Ions and Polar Molecules. J. Chem. Phys., vol. 47, no. 9, Nov. 1, 1967, pp. 3103-3113.

4. Böhme, D. K.; Hasted, J. B.; and Ong, P. P.: Calculation of Interchange Reaction Rates from Transition Times. Chem. Phys. Letters, vol. 1, 1967, pp. 259-262.

5. Gioumousis, George; and Stevenson, D. P.: Reactions of Gaseous Molecule Ions with Gaseous Molecules. V. Theory. J. Chem. Phys., vol. 29, no. 2, Aug. 1958, pp. 294-299.

6. Theard, Lowell P.; and Hamill, William H.: The Energy Dependence of Cross Sections of Some Ion-Molecule Reactions. J. Am. Chem. Soc., vol. 84, no. 7, Apr. 5, 1962, pp. 1134-1139.

7. Moran, Thomas F.; and Hamill, William H.: Cross-Sections of Ion-Permanent-Dipole Reactions by Mass Spectrometry. J. Chem. Phys., vol. 39, no. 6, Sept. 15, 1963, pp. 1413-1422.

8. Dugan, John V., Jr.; and Magee, John L.: Semiclassical Approach to Capture Collisions between Ions and Polar Molecules. NASA TN D-3229, 1966.

9. Dugan, John V., Jr.; Rice, James H.; and Magee, John L.: Calculation of Capture Cross Sections for Ion-Polar-Molecule Collisions Involving Methyl Cyanide. NASA TM X-1586, 1968.

10. Dugan, J. V., Jr.; Rice, J. H.; and Magee, J. L.: On the Nature of Ion-Molecule Collisions. Chem. Phys. Letters, vol. 2, no. 4, Aug. 1968, pp. 219-222.

11. Rapp, Donald; and Francis, W. E.: Charge Exchange between Gaseous Ions and Atoms. J. Chem. Phys., vol. 37, no. 11, Dec. 1, 1962, pp. 2631-2645.

12. Kannenberg, Robert G.: Cinematic - FORTRAN Subprograms for Automatic Computer Microfilm Plotting. NASA TM X-1866, 1969.

NASA-Langley, 1969 —— 24 E-5091